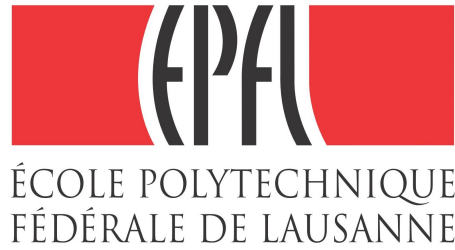


---

# Bachelor Thesis

## School of Life Sciences and Technology

---



at the  
Laboratory for Soft Bioelectronics Interfaces  
Center for Neuroprosthetics, EPFL  
Prof. Stéphanie P. Lacour

## **Functionality analysis of the e-dura flexible micro-ECoG implant for brain-computer interfaces**

By  
Matthias Chinyen Tsai

Lausanne  
September 2014

## Table of Contents

1. Abstract.....	3
2. Introduction.....	4
2.1. Electrocorticography.....	4
2.2. A micro-ECoG implant.....	5
2.3. Evaluation of the potential of e-dura for BCI implementation.....	5
3. Methods.....	6
3.1. Microfabrication of the e-dura implant.....	6
3.2. In vivo experiments.....	7
3.3. Signal processing.....	7
3.3.1. Spectrum of frequencies.....	9
3.3.2. Averaged spectrogram patterns.....	9
3.3.3. Variance analysis of locality (VAL).....	10
4. Results.....	11
4.1. Frequency spectra.....	11
4.2. Characteristic spectrogram patterns.....	15
4.3. Variance analysis of locality.....	20
5. Discussion.....	23
5.1. Frequency spectra.....	23
5.2. Spectrogram patterns.....	24
5.3. Variance analysis of locality.....	25
5.4. E-dura's potential for BCI.....	26
5.5. Future studies.....	26
6. Acknowledgements.....	27
7. References.....	28
8. List of Figures.....	31

## 1. Abstract

This bachelor's thesis aims to evaluate the functionality of the e-dura flexible micro-ECoG design proposed by Arthur E. Hirsch (Laboratory for Soft Bioelectronics Interfaces, EPFL) and its potential for implementation into brain-computer interfaces (BCI). This was done by analyzing the electrocorticographic (ECoG) signal recorded by e-dura in three different rats. The analysis consisted of the comparison of frequency spectra and spectrograms of the recorded ECoG signal correlated with different types of data as well as the development of a variance analysis of locality (VAL) technique in order to measure the similarity of the ECoG signals depending on the spatial localization of the recording electrodes.

The findings showed that e-dura could reliably record ECoG signals for a long period of time and that the inter-electrode distance of 750 µm could be exploited and deliver highly local brain signal measurements. These evidences supported that e-dura could be used in high performance BCI.

## 2. Introduction

In the last few years, BCI have experienced an increased interest thanks to some recent successful implementations into neuroprosthetic technologies. The pioneering work of José del R. Millán and his Lab - the design of a brain-controlled wheelchair (Carlson and Millán, 2013) - is a good example of the results that can be achieved with modern technologies. Like most other BCIs, the brain-controlled wheelchair is based on electroencephalography (EEG), which has become a method of choice for the purpose of modern neuroprosthetic implementations (Wilson et al., 2012). The reason for this is the low invasiveness of the technology. Because EEG electrodes are placed on the scalp of the subjects, it does not require surgery nor can it damage the brain. The possibility to incorporate EEG electrodes onto a cap that can be rapidly put on and taken off at will (Light et al., 2010), also makes it a convenient solution for neuroprosthetic purposes. Despite these advantages, EEG technology has been shown to have many limitations regarding its spatial resolution, frequency range (Mak and Wolpaw., 2009) and signal-to-noise ratio (Smith et al., 2013).

### 2.1. Electrocorticography

It has been proposed that ECoG could be a promising alternative to EEG for BCI implementations (Leuthard et al., 2004). While EEG signal is specific only up to several centimeters and spans frequencies in the range of 0-40 Hz (Schalk, 2012), ECoG has a spatial resolution going down to 1.25 mm (Freeman et al., 2000) and can measure frequencies up to 500 Hz (Gaona et al., 2011). Another advantage of ECoG over EEG is the greater signal-to-noise ratio (Hill et al., 2012). This is due to the fact that the signal recorded by EEG is blurred and attenuated by the tissue layers separating the electrodes from the brain (Buzáki et al., 2012); these include the scalp, the skull and the cerebrospinal fluid (Da Silva and Van Rotterdam, 2005).

On the other hand, ECoG still has a main disadvantage compared to EEG. The relative invasiveness related to the location of the ECoG electrodes under the skull is the most critical feature of the technology. Nevertheless it remains less invasive than intracortical electrode, which are known to induce local damage of neurons, microhemorrhages and acute reactive responses following to their implantation (Fernández et al., 2014). Intracortical electrodes are therefore currently not reliable for long term applications (Cheung et al., 2007; Wooley et al., 2013). For these reasons the current consensus has been that epicortical electrodes (subdural or epidural; see Fig.1) would have better chances to achieve a safe standard for chronic implementations. While optimization of intracortical electrode arrays is currently undertaken to render them as flexible and safe as possible (Xiang et al., 2014), the focus of this thesis is centered on electrocorticographic implants recording potentials from the surface of the cortex.

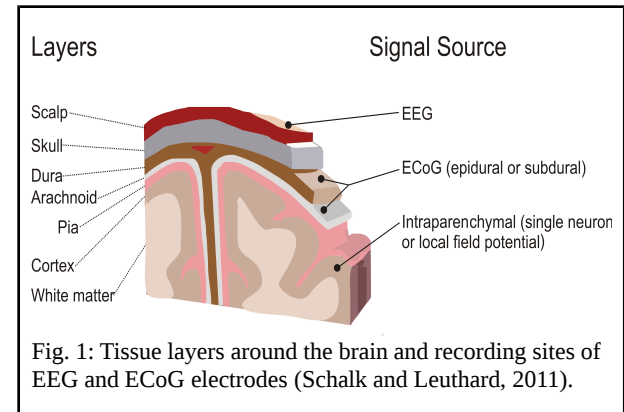


Fig. 1: Tissue layers around the brain and recording sites of EEG and ECoG electrodes (Schalk and Leuthard, 2011).

## 2.2. A micro-ECoG implant

In order to develop an ECoG based BCI, it is first necessary to improve ECoG technology and develop a design that is reliable, stable and safe for chronic implants. Today, the side effects and long term stability of ECoG still remain insufficiently studied to allow ECoG technologies to be clinically tested in humans over a long period of time. The reason for this is that ECoG has almost exclusively been used on patients prior to epileptic surgical resectioning and that its application has strictly been reduced to the duration of its clinical requirements (Schalk and Leuthard, 2011). In order to fulfill the safety requirements, necessary to allow long term clinical trials, it is crucial for the implant to be as thin and flexible as possible. Such features allow the implant to accommodate brain curvature and maintain close contact between the microelectrodes and the brain; furthermore they minimize movement related tissue stress due to motion of the brain within the skull (Buzáki et al., 2012). For the purpose of high performance BCI, it is also important to magnify the spatial resolution of the micro-ECoG implant and thus maximize the specificity and the information content of the recorded signal. To achieve this, the implant has to be miniaturized, and the inter-electrode distance narrowed down to come as close as possible to the postulated optimum spacing of 1.25 mm (Freeman et al., 2000).

To cope these challenges, Arthur E. Hirsch from the Laboratory for Soft Bioelectronic Interfaces at EPFL designed and microfabricated flexible micro-ECoG implants. This new ECoG design was named e-dura.

## 2.3. Evaluation of the potential of e-dura for BCI implementation

E-dura was tested on rats to assess its functionality *in vivo*. It was then necessary to collect the recorded ECoG data and analyze it, in order to estimate the performance of the implant. The focus was made on its potential for BCI implementations. This required to evaluate the spatial resolution and the stability of e-dura over a longer period of time. Another important characteristic is the impedance of the electrodes. A lower impedance electrode improves the signal quality and diminishes the noise content, thus enhancing the signal-to-noise ratio (Castagnola et al., 2014). It is therefore also very informative to assess the change in impedance of the electrodes over time.

### 3. Methods

Before further reading, it should be noted that the e-dura microfabrication as well as the in vivo experiments were mainly carried out by Arthur E. Hirsch, while the post-experimental study including the signal processing and statistical analysis was performed by Matthias Chinyen Tsai. The microfabrication and experimental procedures were conducted in various facilities of the Swiss Federal Institute of Technology in Lausanne (EPFL).

#### 3.1. Microfabrication of the e-dura implant

The electrodes are embedded in a thin polydimethylsiloxane (PDMS) stripe, which is known to be biocompatible and to only induce mild and temporary inflammatory reactions when implanted (Bélanger and Marois, 2001). The electrode sites are coated with a conductive blend of platinum nano-micro particles and PDMS to cover the chromium and gold films that relay the electrical signal through the PDMS stripe.

This design is achieved by first taking a 3" silicon carrier wafer pre-coated with polystyrene sulfonic acid (as a water soluble release layer) and spin-coating it with a 100 $\mu$ m thick layer of PDMS before curing the PDMS substrate at 80°C. Next, layers of chromium and gold films of respectively 5 and 35 nm are laminated on the PDMS substrate by shadow mask thermal evaporation to form the tracks relaying the signals from the 9 microelectrodes. In parallel a triple PDMS stack is manufactured consisting of a 5 mm thick slab and two 20  $\mu$ m thick layers all separated by release coatings that will allow them to be separated at a later stage. The two thin 20  $\mu$ m thick PDMS layers are simultaneously punctured at the locations where the electrode sites would be situated using a hollow glass capillary. The two pieces are then covalently bound to each other after aligning the punctured holes with the electrode sites and the thick PDMS slab is peeled off. Finally, the electrode sites are coated with customized platinum-silicone composite before the silicon carrier wafer is removed, releasing the 140  $\mu$ m thick e-dura implant.



Fig. 2: Flexible e-dura implant designed and manufactured by Arthur Hirsch.

### 3.2. In vivo experiments

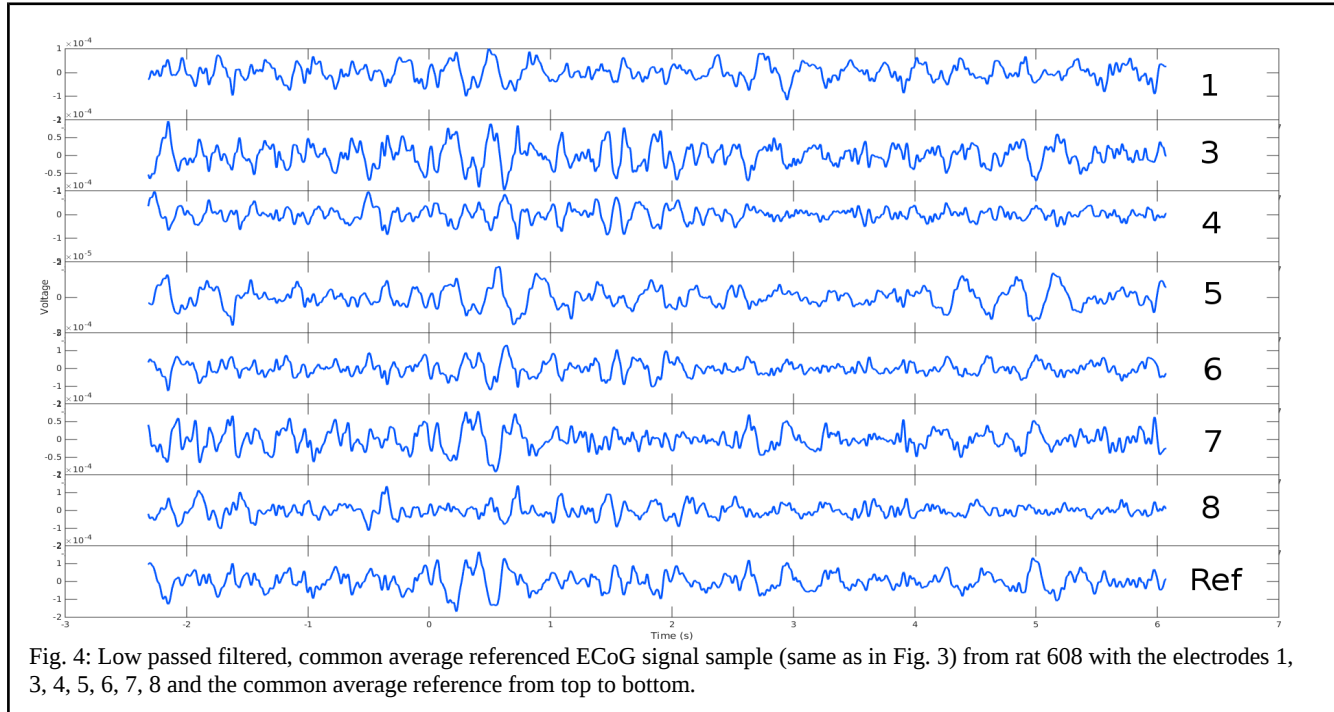
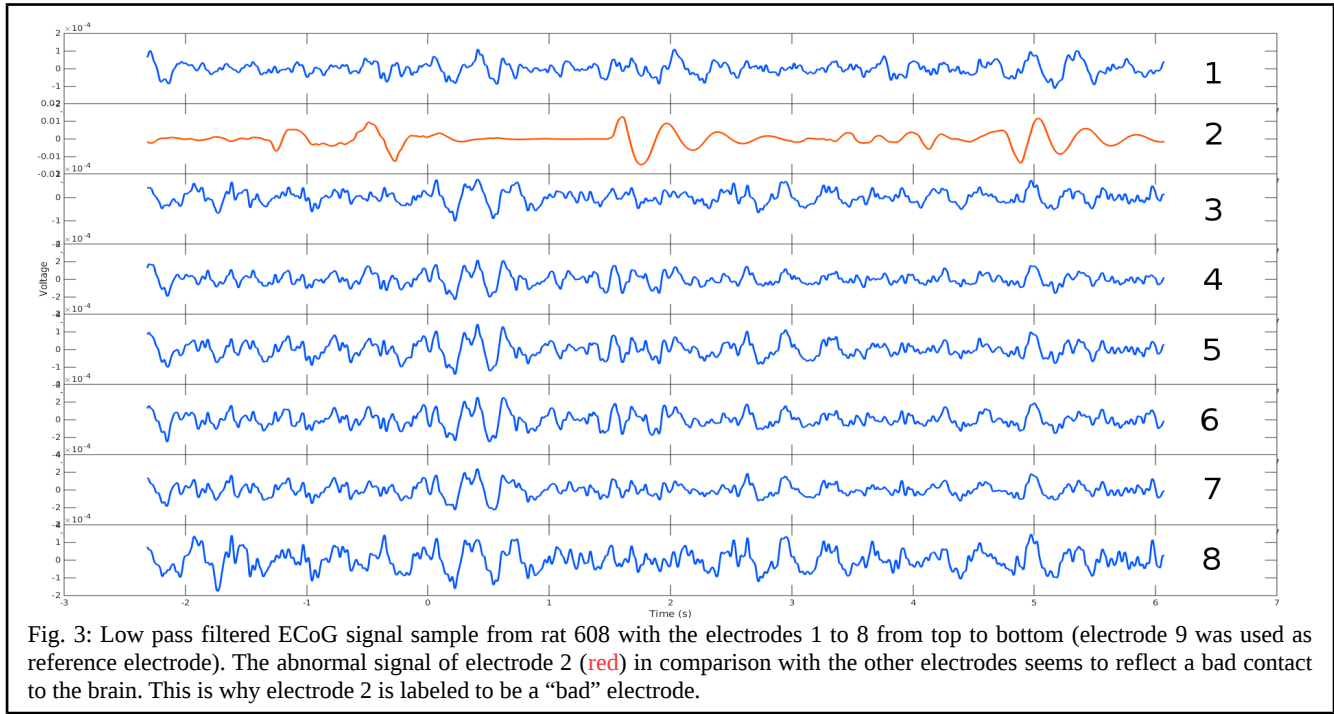
After the e-dura prototype had been successfully fabricated and tested in vitro, the next step was a long term in vivo study. Since it could not be tested on humans, it was decided to surgically implant the e-dura prototype subdurally on the left motor cortex of three different rats. The brain activity of each individual was then measured during the performance of different experimental tasks. One task was to abruptly start a run for a certain distance and stop before remaining quiet, the whole process taking place on a flat surface without any obstacles. The second experiment was very similar to the first, with the only difference that the rats had to run over a horizontal ladder. This would be more difficult and demand additional concentration. More importantly the rat would sometimes slop through a hole of the ladder with one foot, which would result in stumbling. Each experiment was repeated by each rat several times on three different days: 7, 21 or 55 days after implantation of e-dura. The brain activity was monitored throughout the experiments with the flexible micro-ECoG implants, and the signals as well as a video of the experiments were recorded.

E-dura used one of its electrodes as reference and used the recorded electrical potential of this electrode to compute the voltage difference to the recorded potentials of the other electrodes.

### 3.3. Signal processing

The data was collected and analyzed by first reviewing the video records of the experiments and tagging different types of events that were related to the behavior of the rats and could be correlated with the recorded ECoG signals. The specific events were: the onset of a run (“start”), the end of a run (“stop”), the beginning of quiet behavior, during which the rat moved very little (“start passive”), the end of a quiet behavior, after which the rat moved more actively (“stop passive”) and the stumbling of a rat resulting from an improper move of the hind leg and falling through a gap of the ladder with either the left or the right hind foot. These events were tagged on a program allowing their exact moment of occurrence to be retrieved after the complete set of data had been imported on Matlab 8.3 (The MathWorks, Inc., R2014b release).

Before any signal processing was performed, the recorded ECoG signal was re-referenced by using a technique called common average referencing. For this, it is first necessary to figure out, which electrodes of the implant might be corrupted and might have either had a bad contact to the brain or been subject to some strong noise. The screening for these bad electrodes was made subjectively by looking at the recorded ECoG and trying to detect electrodes that seemed to record abnormal signals (see Fig. 3). After the corrupted electrodes had been determined, the average of the ECoG record over all uncorrupted electrodes was taken and subtracted from the signal of each individual electrode as described by Dien (1998) (see Fig. 4).



### 3.3.1. Spectrum of frequencies

By computing the fast Fourier transforms of the recorded ECoG signals and averaging their frequency amplitudes for each day on which the ECoG was recorded, it is possible to roughly estimate the change in impedance of the electrodes throughout time. This can be done by comparing the overall frequency amplitudes over the different days, and because an increase in impedance results in a decrease of overall amplitude. This methodology is far from precise, since it is sensitive to many variable factors that can influence the average frequency amplitudes without the direct involvement of impedance changes. If on one day a rat had been more active than on another, its brain activity would be higher and thus the computed frequency amplitudes would be greater. By analyzing the data carefully though, it is possible to obtain a qualitative estimate of the impedance changes. In an attempt to attenuate the unpredictability and irregularity of the rat's behavior throughout the experiments, only the ECoG signals were evaluated, during which the rat was either quiet or running. By choosing one of these behaviors as a standard, the associated brain activity should stay constant and relatively consistent over the trials.

Due to the shortage of data during which the rat was quiet or "passive", this method could only be completed for the ECoG records, during which the rats were running or "active".

### 3.3.2. Averaged spectrogram patterns

In order to implement BCI technologies, it is necessary to characterize certain brain signals and correlate them with specific tasks, behaviors or cerebral activities. With this idea in mind, it was attempted to find out the characteristic spectrogram patterns around certain key moments of the rats' behavior. If it could be shown that these differed between the different electrodes, it would also display an indicator for the spatial resolution of the implant and the individual information content that every single electrode could offer. The events investigated were "start", "stop" and the stumbling of the left or the right foot.

First, ECoG signals of 3 seconds duration windows around the occurrence of the chosen events were extracted. Next the Spectrograms of these samples were computed by taking many short time Fourier transforms at different time points with window sizes of approximately 0.34 s over a range of 6-300 Hz (omitting the power line frequency between 45 and 55 Hz). This was done for all available samples. Finally, the mean spectrograms of each type of event were computed for each uncorrupted electrode in order to average out any noise related contribution. The frequency amplitudes were then renormalized by dividing every element of the power density matrix by the average power of the same frequency and converting the output in decibel before plotting the resulting data onto a spectrogram.

Since the e-dura implants had been implanted on the left hemisphere of the rat's motor cortex, it would be especially interesting to compare the resulting patterns from stumbling events of the right and the left foot. Unfortunately, this comparison would reveal itself to be incomplete due to the shortage of left stumbling events that was limited to 7 cases at most, which is insufficient to produce a statistically significant result. The other types of events fortunately occurred more often and delivered reliable results.

### 3.3.3. Variance analysis of locality (VAL)

Since the average spectrogram patterns can only provide a qualitative insight on the specificity and the spatial resolution of the electrodes, it was necessary to conduct another analysis in order to better estimate how distinct the ECoG recordings of the single electrodes could be from each other.

This analysis is based on the following hypothesis: since nearby electrodes should record more similar signals than further distanced electrodes, the variance of the difference between two ECoG signals should be positively correlated with the distance between the two recording electrodes. Following this train of thought, every combinatorially possible difference between the recorded signal of two uncorrupted electrodes ( $i$  and  $j$ ) was calculated before computing their variances. This was done for every recorded samples ( $k$ ) before the mean of these values (VAL) was computed for each combination of electrodes.

$$VAL_{ij} = \frac{1}{n} \sum_{k=1}^n \text{variance}(\text{electrode}_i^k - \text{electrode}_j^k) \quad (1)$$

In order to keep track of this big amount of results and facilitate the overall evaluation of this data, VAL maps were laid out using a specific color code and positioning the displayed VALs in an intuitive manner on a grid.

## 4. Results

Before the results of the data analysis are presented, it is important to describe the brain condition of the three rats, in which e-dura was implanted, 60 days after implantation of e-dura. One of them had developed an infection during the experiments and revealed a hole comprising 50% of its left hemisphere. The two others showed signs of light but non-negligible brain herniations. It was therefore decided to only analyze the data of the rats with the herniations and to omit the data from the rat that showed damage on a complete hemisphere.

The electrode 2 of rat 608 and the electrodes 5 and 8 of rat 610 were found to be corrupted and were therefore not included in the analysis nor used for the average referencing.

### 4.1. Frequency spectra

The mean frequency spectrum of the complete data of either rat 608 or 610 both show similar frequency amplitudes between the recordings made 7 and 21 days after implantation (respectively P7 and P21 data), while the amplitude of the recordings made 55 days after implantation (P55 data) is greater than the P7 and P21 amplitudes by approximately a factor 10 (see Fig. 5 and 6).

Since the amount of “passive” data was very limited, its frequency spectrum could only be plotted for rat 608, which itself had only produced between 3 and 15 passive samples on a single day and therefore didn't deliver a statistically strong result. Fortunately, the rats generated sufficient active data to yield results with more significant statistical significance. There were between 13 and 30 active samples per day for each rat. The computed results of the active and passive data are qualitatively similar (see Fig. 6, 7 and 8). They indicate a significant increase in amplitude between 21 and 55 days post implantation. An interesting specific feature of the active data is that the frequency spectra of both rats (608 and 610) show a decrease in signal amplitude between P7 and P21 that can't be seen in the passive or the general data (or very remotely from the general data of rat 610).

The depression observed around 50 Hz is due to the filtering out of the power line frequency.

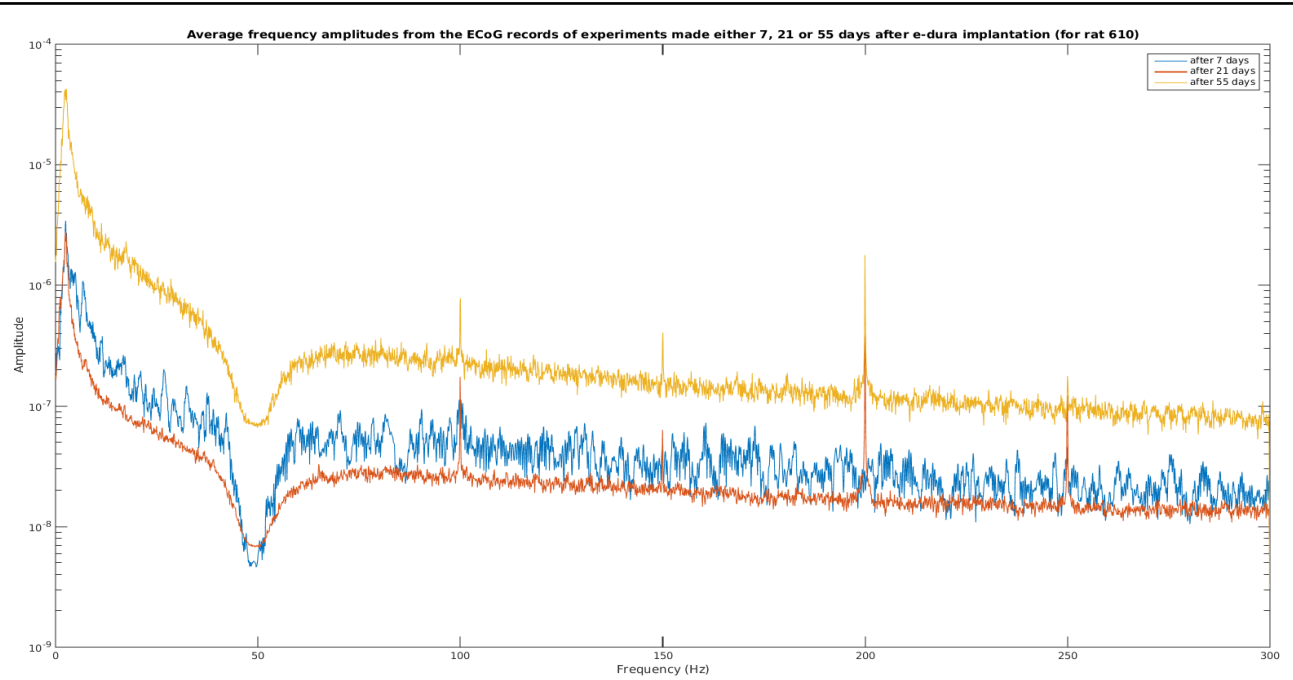


Fig. 5: Comparison of the frequency spectra from the data collected 7, 21 or 55 days after the implantation of the e-dura implant. This is the result of the fast Fourier transforms of the recorded ECoG signals from rat 610 being averaged over the electrodes and over the trials made on the respective days.

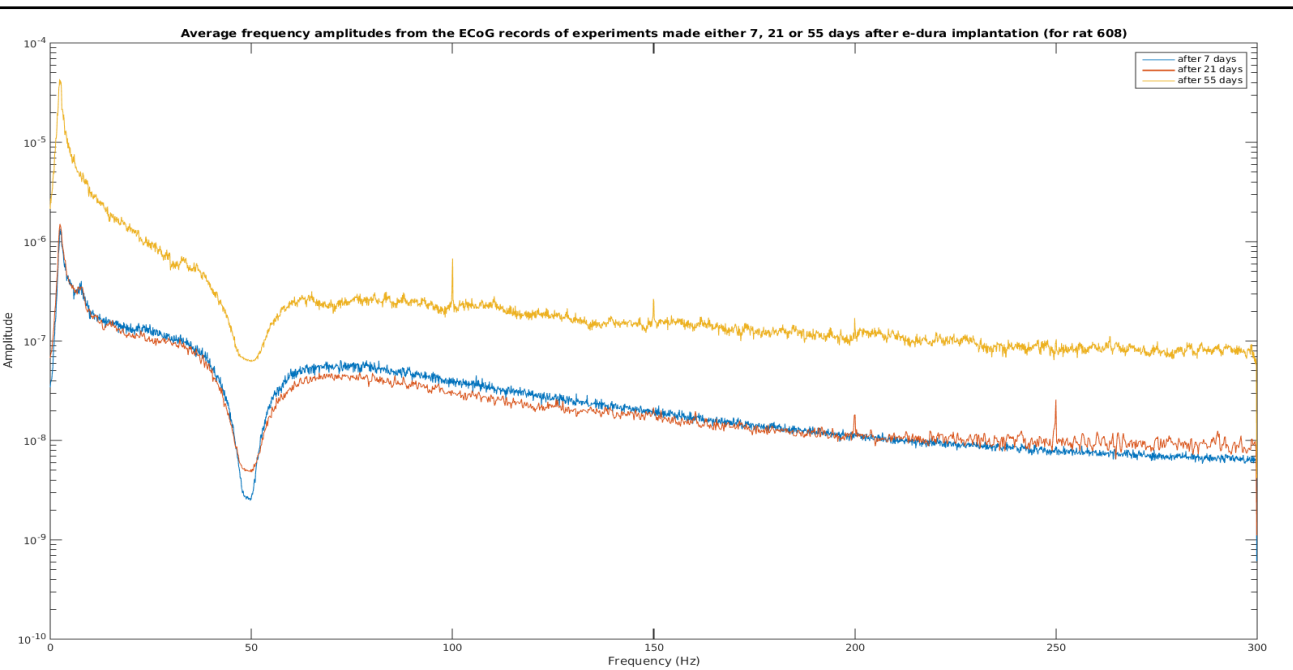


Fig. 6: Comparison of the frequency spectra from the data collected 7, 21 or 55 days after the implantation of the e-dura implant. This is the result of the fast Fourier transforms of the recorded ECoG signals from rat 610 being averaged over the electrodes and over the trials made on the respective days.

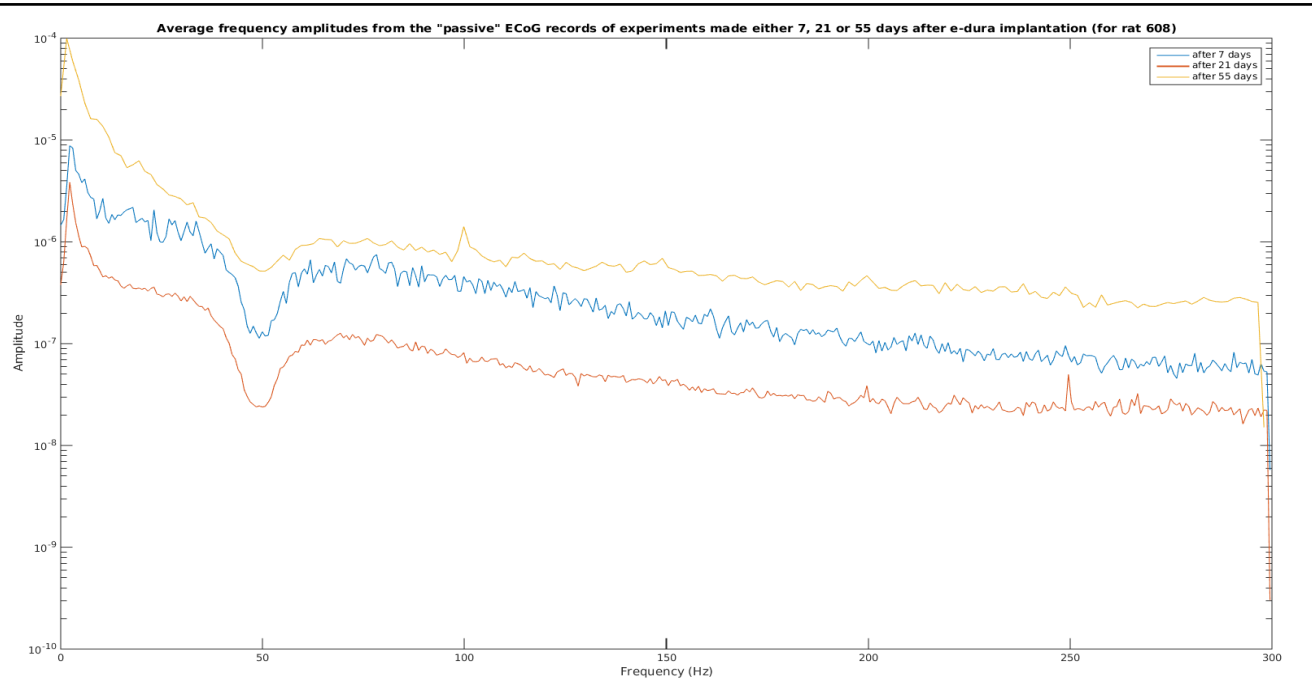


Fig. 7: Comparison of the frequency spectra from the data collected 7, 21 or 55 days after the implantation of the e-dura implant. This is the result of the fast Fourier transforms of the ECoG signals recorded while rat 608 was still ("passive"), averaged over the electrodes and over the trials made on the respective days.

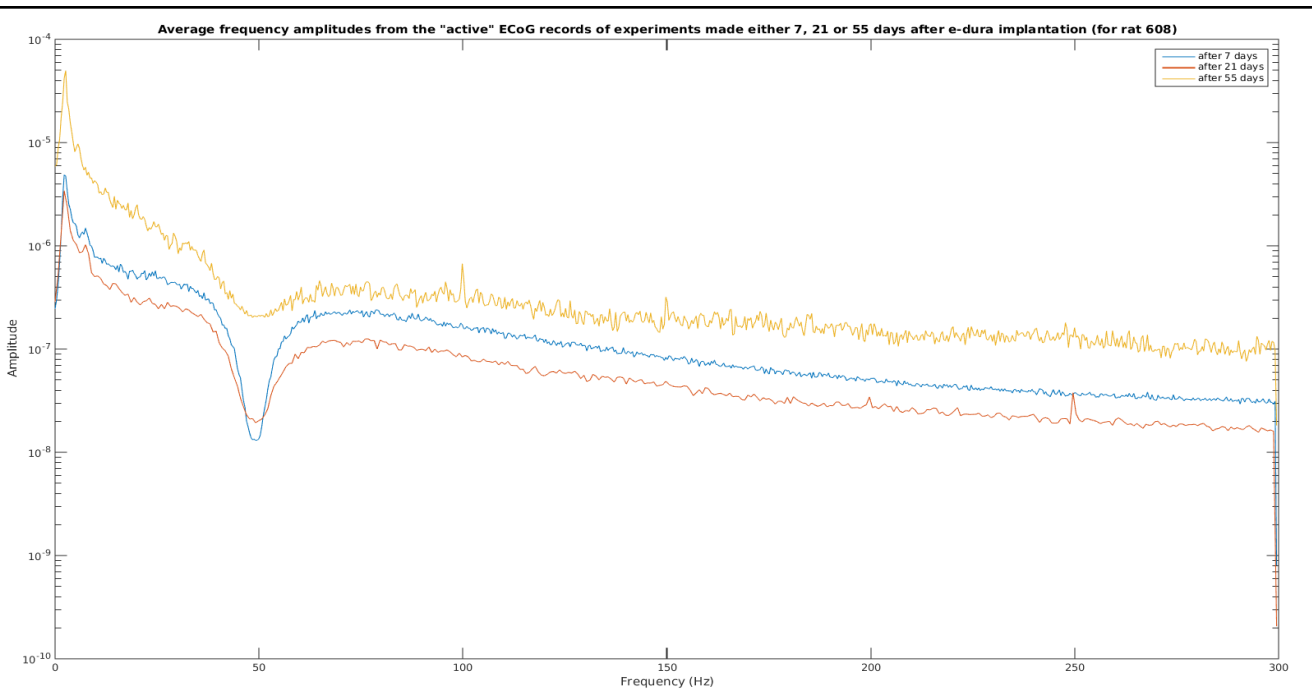
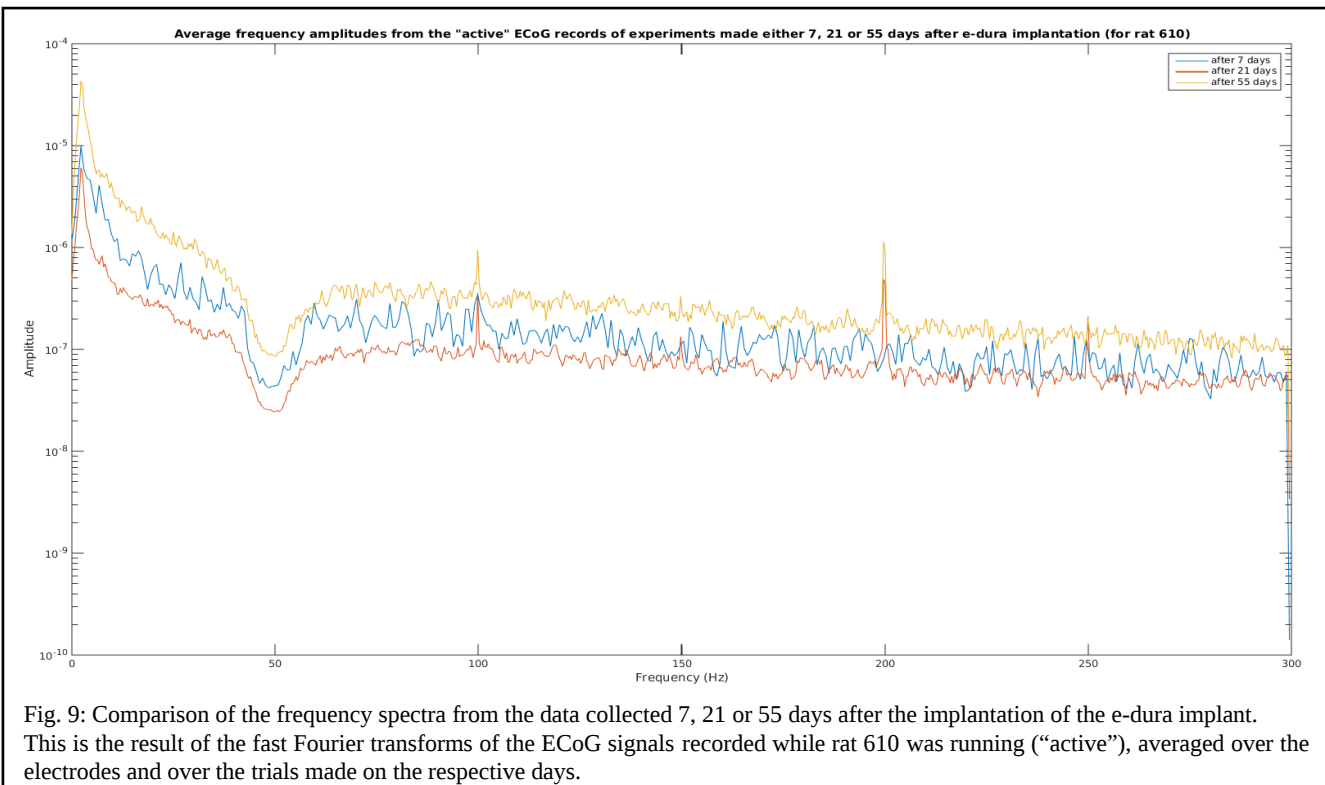


Fig. 8: Comparison of the frequency spectra from the data collected 7, 21 or 55 days after the implantation of the e-dura implant. This is the result of the fast Fourier transforms of the ECoG signals recorded while rat 608 was running ("active"), averaged over the electrodes and over the trials made on the respective days.



## 4.2. Characteristic spectrogram patterns

The averaged spectrograms for rat 608 reveal distinct patterns for each type of event. On the patterns of the events “start” and “stop”, it is quite noticeable how accurate the moment of sudden rise or fall of overall frequency amplitude corresponds to the time of the event (at 0 sec) tagged on the plots (see Fig. 10 and 11). Slight differences between the single patterns for each electrode are noticeable. Electrode 8 even seems to appreciably stick out of the main picture due to a somewhat more polarized pattern.

When looking at the events of right and left foot stumbling (see Fig. 12 and 13), it is interesting to note the discrepancies between the patterns of the two events. Especially the pattern in the high gamma range between 200 and 300 Hz seems to differ strongly. The bright yellow lines of electrodes 5 and 8 of the left foot stumbling event are probably noise related and shouldn't be taken into account for the interpretation of the results.

Because of scarcity of stumbling events, only the start and stop specific spectrogram patterns of rat 610 were computed. Unfortunately they seem completely dominated by noise related signals and are not proper for any meaningful interpretation (see Fig. 14 and 15). It was attempted to subjectively extract the individual samples that had been subject to noise and repeat the computation without them. Although electrode 4 yields a chaotic and unexpected pattern and the stop event still seems to contain noise related contributions at the very beginning of the signal, the big picture of these new results is satisfying (see Fig. 16 and 17). Especially the stop pattern ostensibly fits the picture laid out by the results from rat 608 by precisely exhibiting a decrease in overall frequency amplitude at t=0s. Perhaps even more interestingly, the contribution of the average referencing technique to remove the global noise from the individual signals is distinctly visible on both of these patterns.

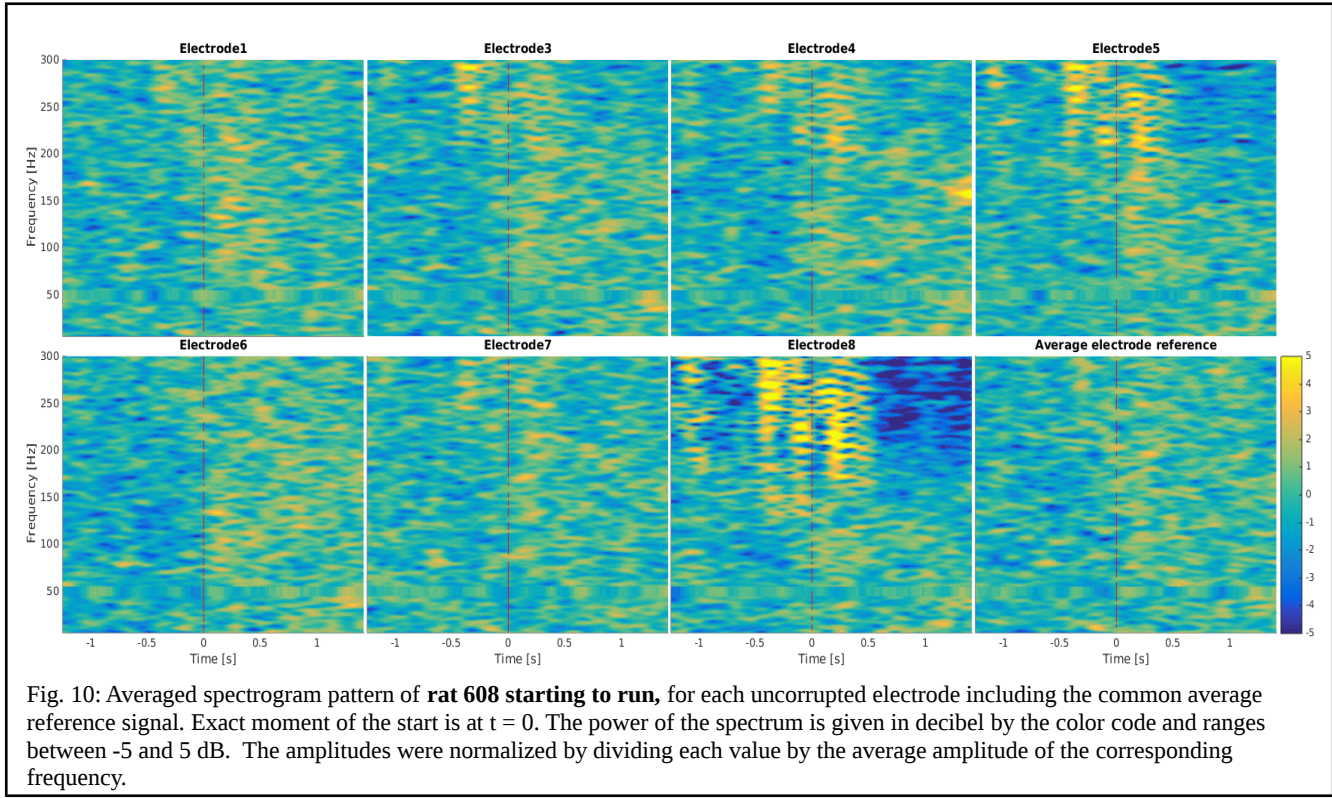


Fig. 10: Averaged spectrogram pattern of **rat 608 starting to run**, for each uncorrupted electrode including the common average reference signal. Exact moment of the start is at  $t = 0$ . The power of the spectrum is given in decibel by the color code and ranges between -5 and 5 dB. The amplitudes were normalized by dividing each value by the average amplitude of the corresponding frequency.

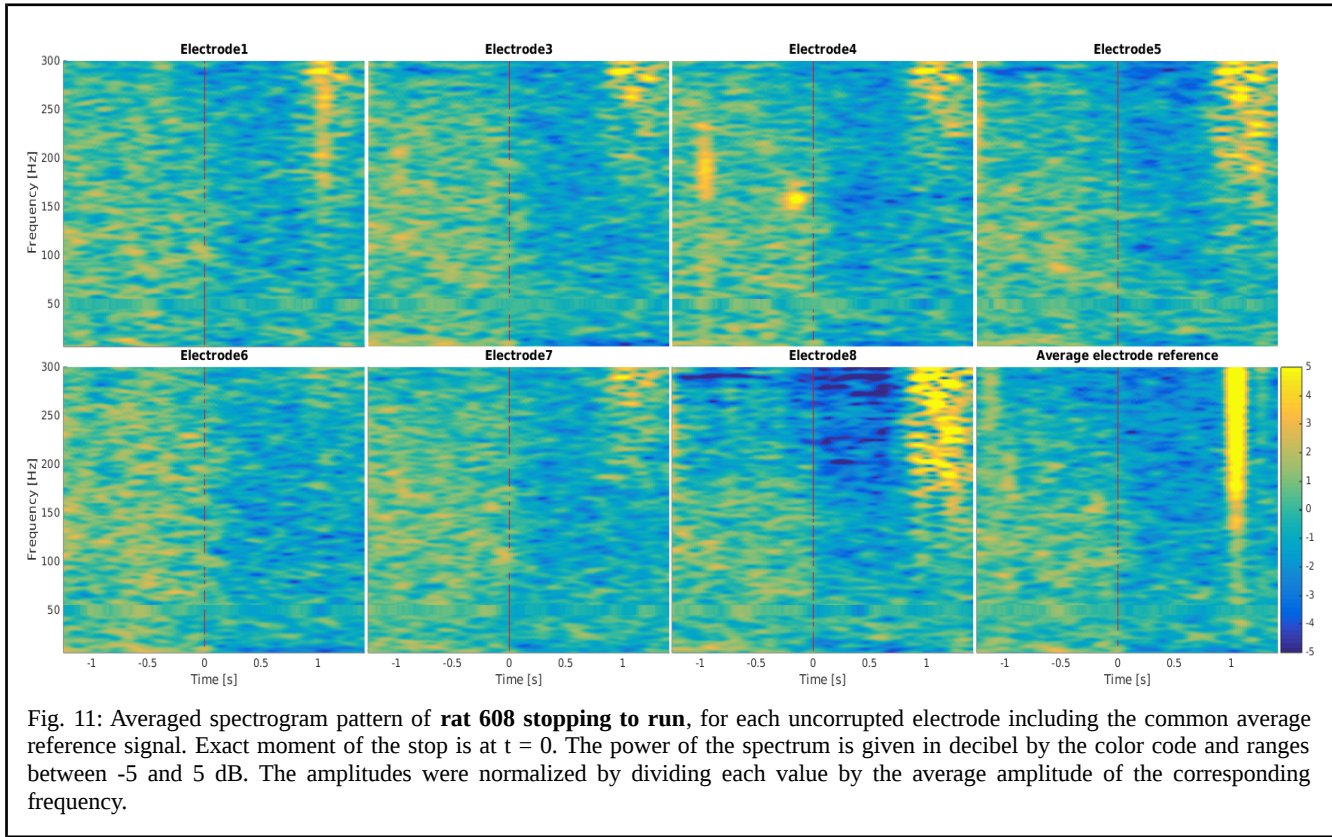
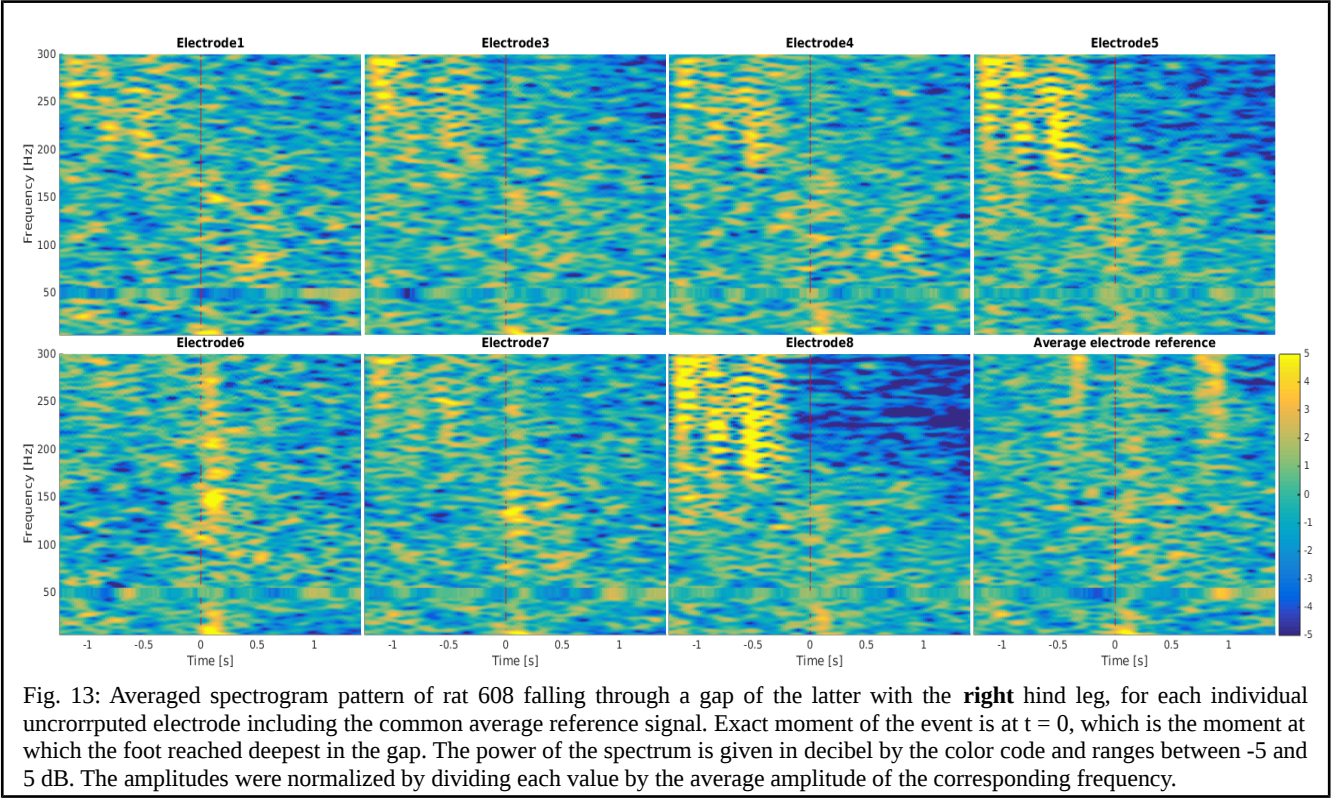
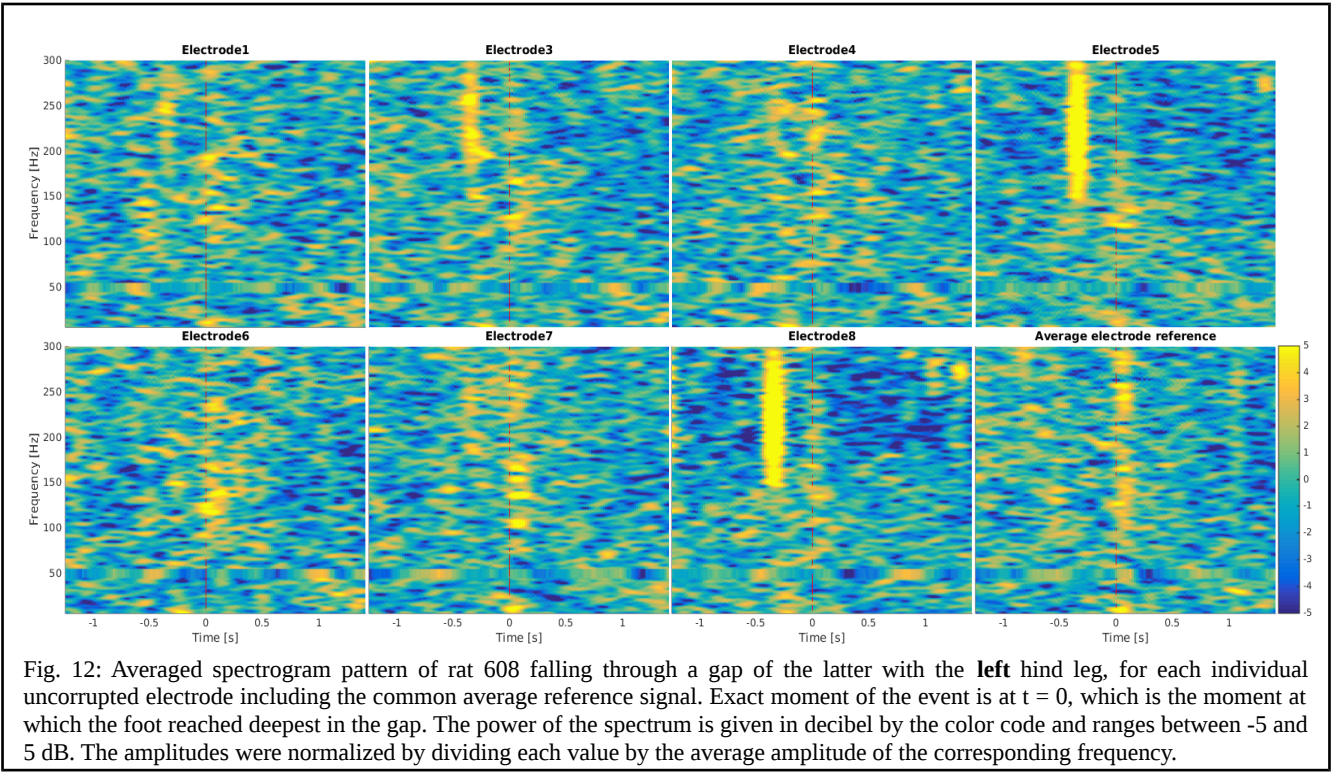
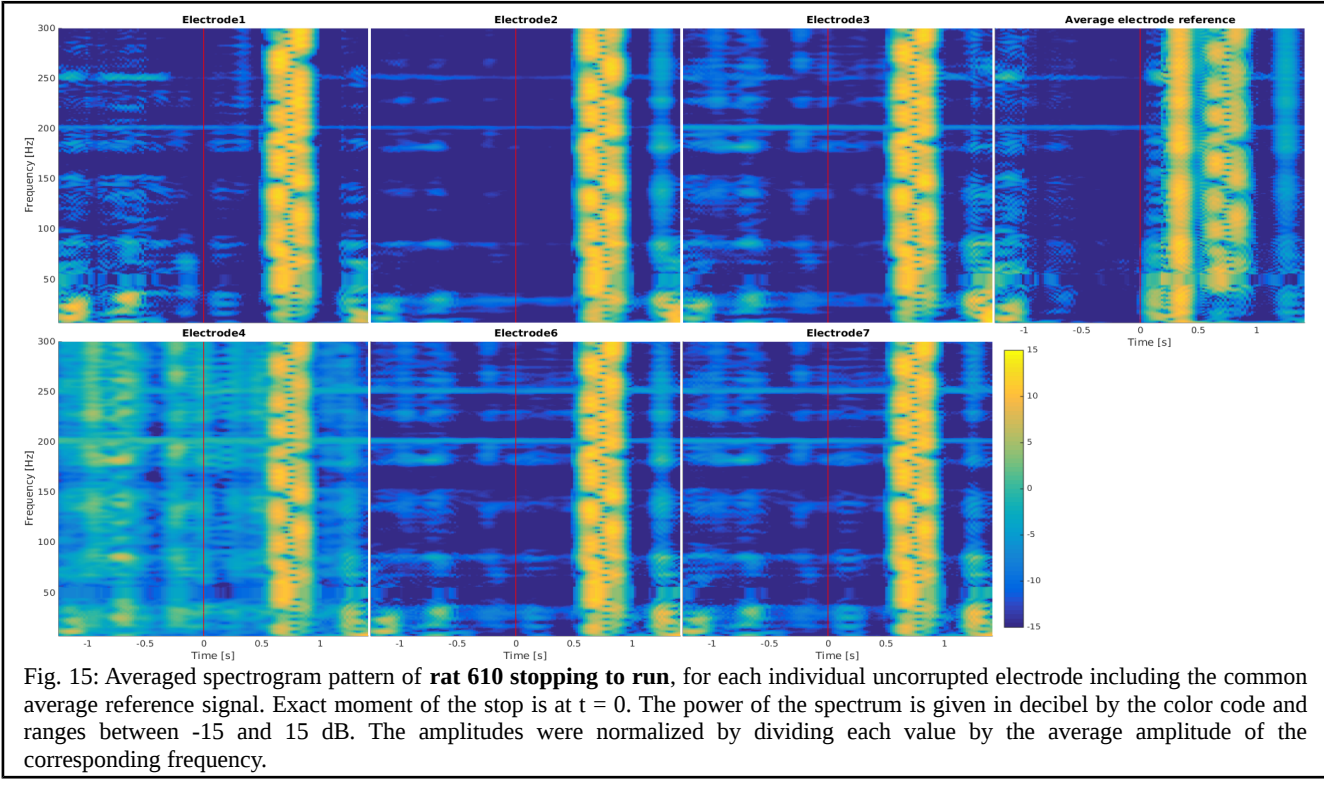
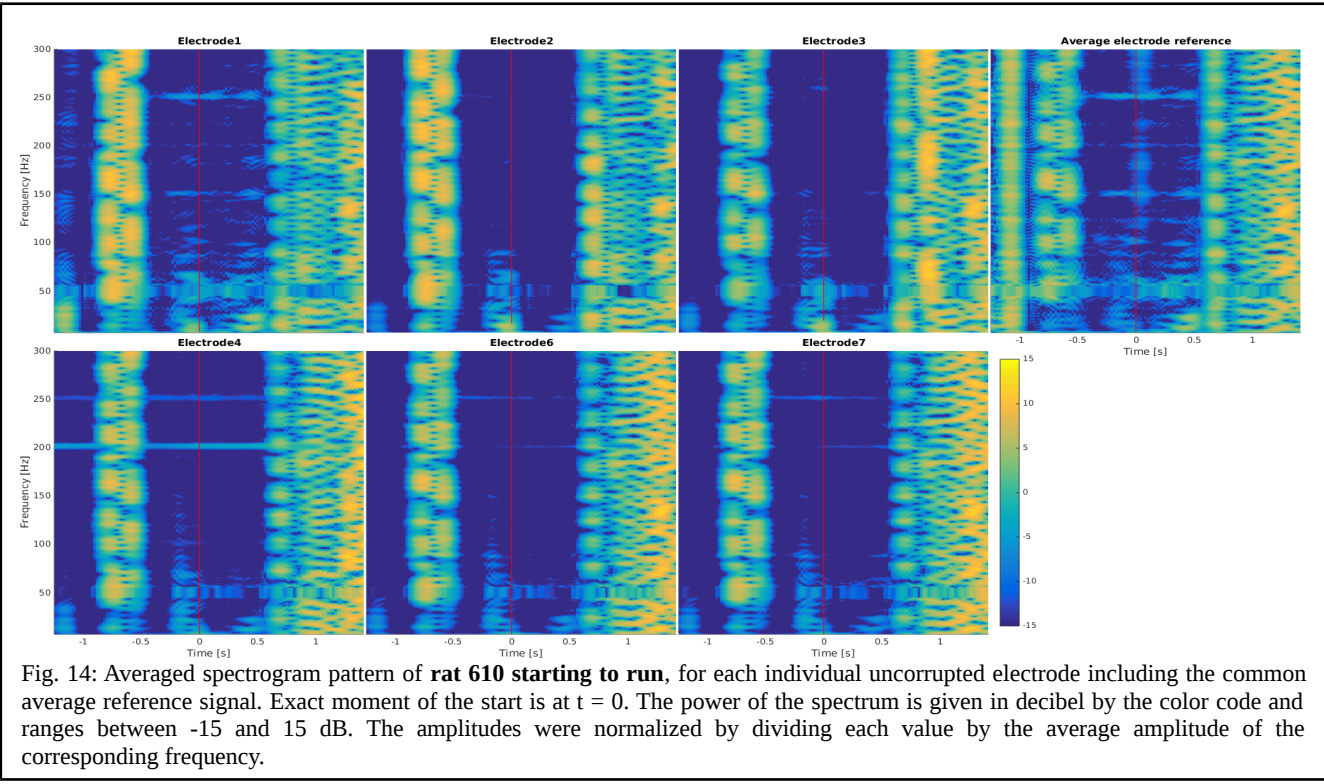


Fig. 11: Averaged spectrogram pattern of **rat 608 stopping to run**, for each uncorrupted electrode including the common average reference signal. Exact moment of the stop is at  $t = 0$ . The power of the spectrum is given in decibel by the color code and ranges between -5 and 5 dB. The amplitudes were normalized by dividing each value by the average amplitude of the corresponding frequency.





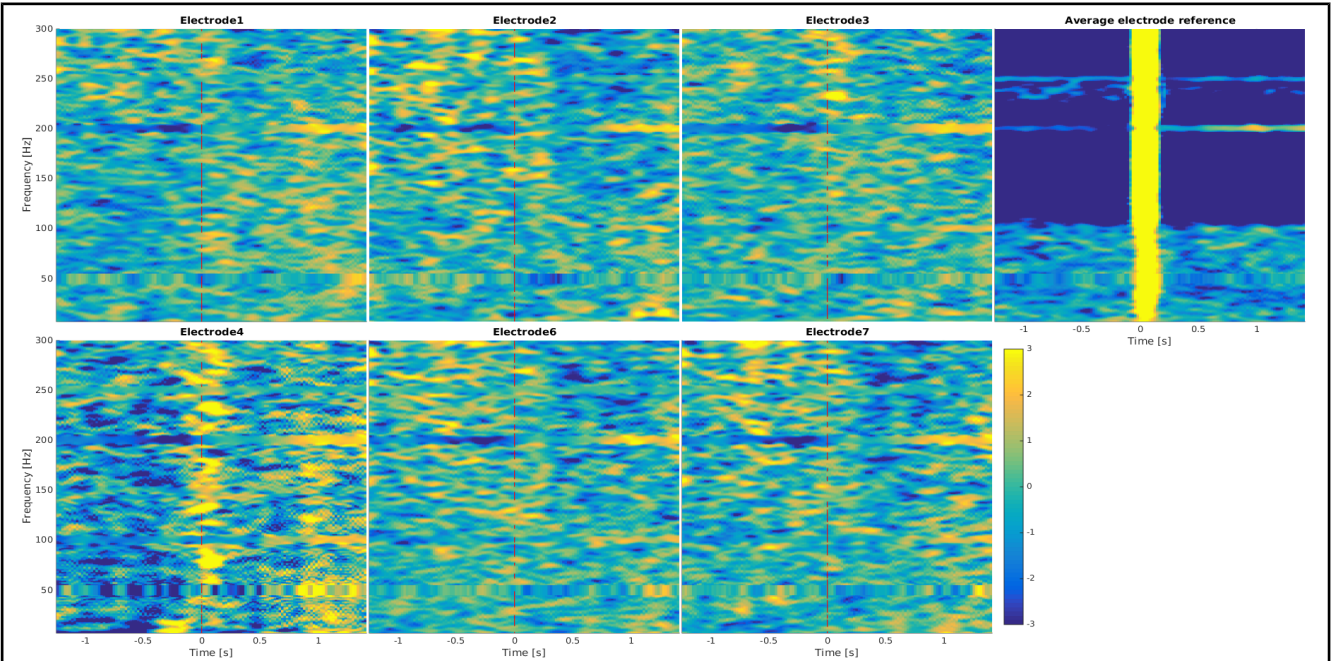


Fig. 16: Averaged spectrogram pattern of **rat 610 starting to run**, for each individual uncorrupted electrode including the common average reference signal. It contains the same data as Fig. 14 with the only difference that some samples were subjectively screened as corrupted and omitted in the computation of this average spectrogram. Exact moment of the start is at  $t = 0$ . The power of the spectrum is given in decibel by the color code and ranges between -3 and 3 dB. The amplitudes were normalized by dividing each value by the average amplitude of the corresponding frequency.

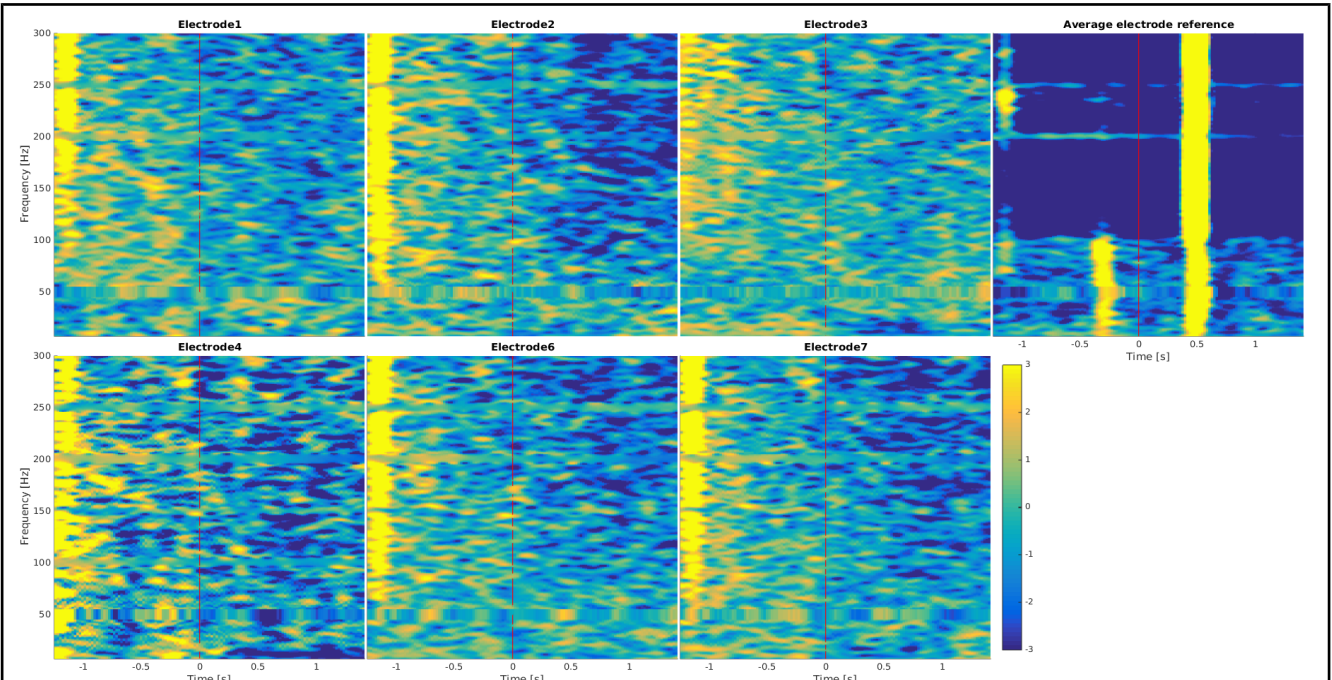


Fig. 17: Averaged spectrogram pattern of **rat 610 stopping to run**, for each individual uncorrupted electrode including the common average reference signal. It contains the same data as Fig. 14 with the only difference that some samples were subjectively screened as corrupted and omitted in the computation of this average spectrogram. Exact moment of the stop is at  $t = 0$ . The power of the spectrum is given in decibel by the color code and ranges between -3 and 3 dB. The amplitudes were normalized by dividing each value by the average amplitude of the corresponding frequency.

### 4.3. Variance analysis of locality

Fig. 16 illustrates the results of variance analysis of locality that include electrode 6 in what will be hereafter referred to as a VAL map. It displays the VAL between each uncorrupted electrode and electrode 6. The redder the color, the bigger the VAL; the yellower, the smaller the VAL. Since the VAL is hypothesized to be positively correlated with the distance between the two electrodes, the color should also become redder the further away the electrodes are apart. In the case of this variance analysis of electrode 6, the hypothesis seems to be confirmed by the results.

Fig. 19 and 20 show the VAL maps of each good electrode of the rats. Each map is localized on grid in such a way that it reflects the position of the concerned electrode on the ECoG implant. The VAL maps of rat 608 perfectly confirm the hypothesis of positive correlation between VAL and the inter-electrode distance with one single peculiarity (see Fig. 19). Electrode 8 (top left) displays a considerably bigger VAL with the other electrodes than what would be expected by only taking into account the other VALs. When looking at the VAL maps focused on electrodes 3 and 7, which are both direct neighbors of electrode 8, one can notice that the VALs of electrode 8 are the biggest on the maps.

A different type of anomaly is yielded by the VAL maps of rat 610 (see Fig. 20). In this case electrode 2 and 3, which are not direct neighbors, seem to have recorded an remarkably similar signal. By looking at their respective VAL maps, it is obvious that their common VAL is much smaller than the ones with closer electrodes, which disagrees with the positive correlation hypothesis between VAL and inter-electrode distance.

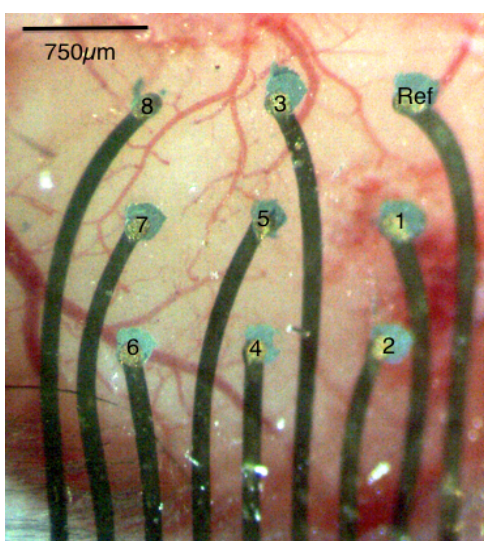
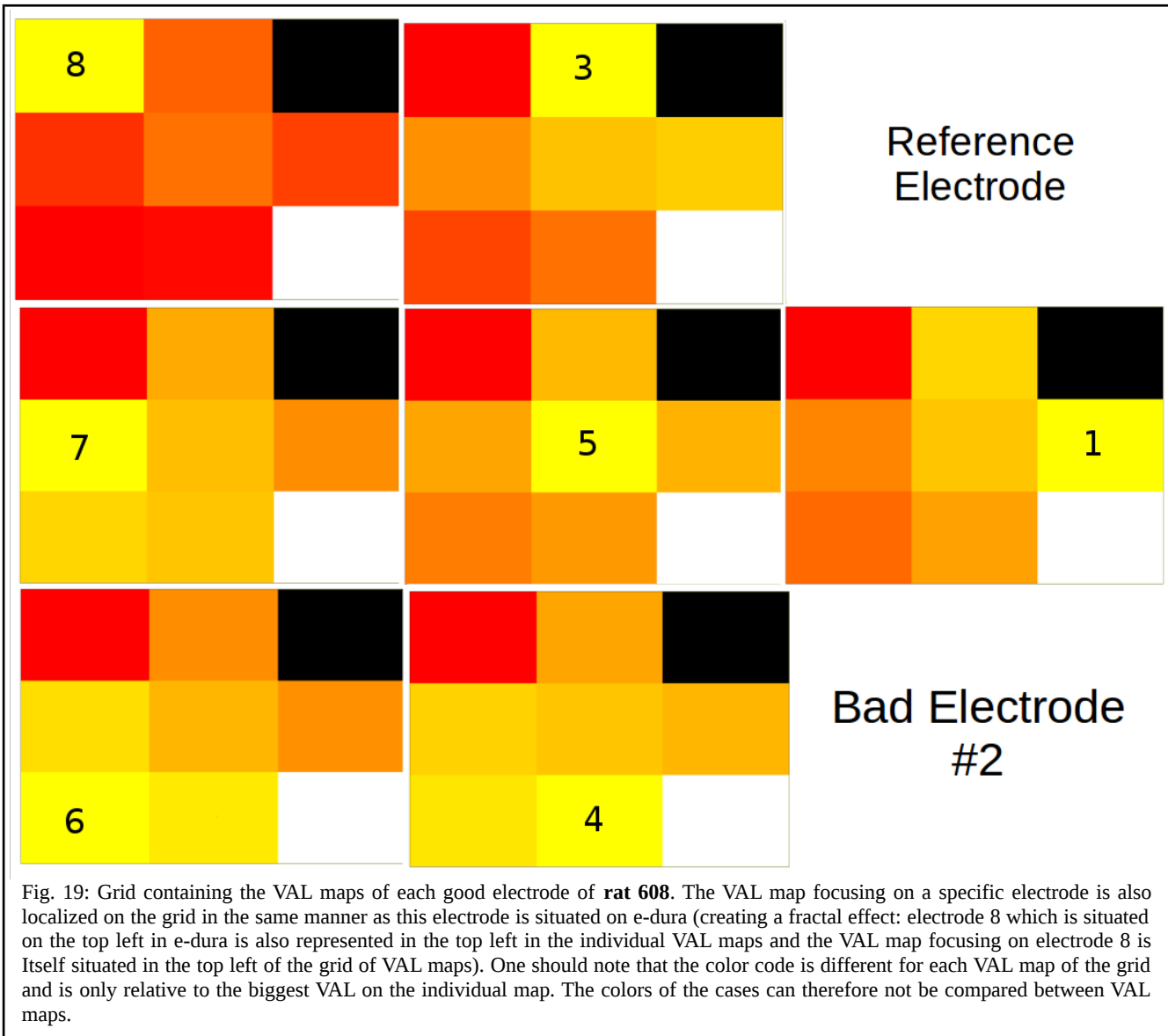
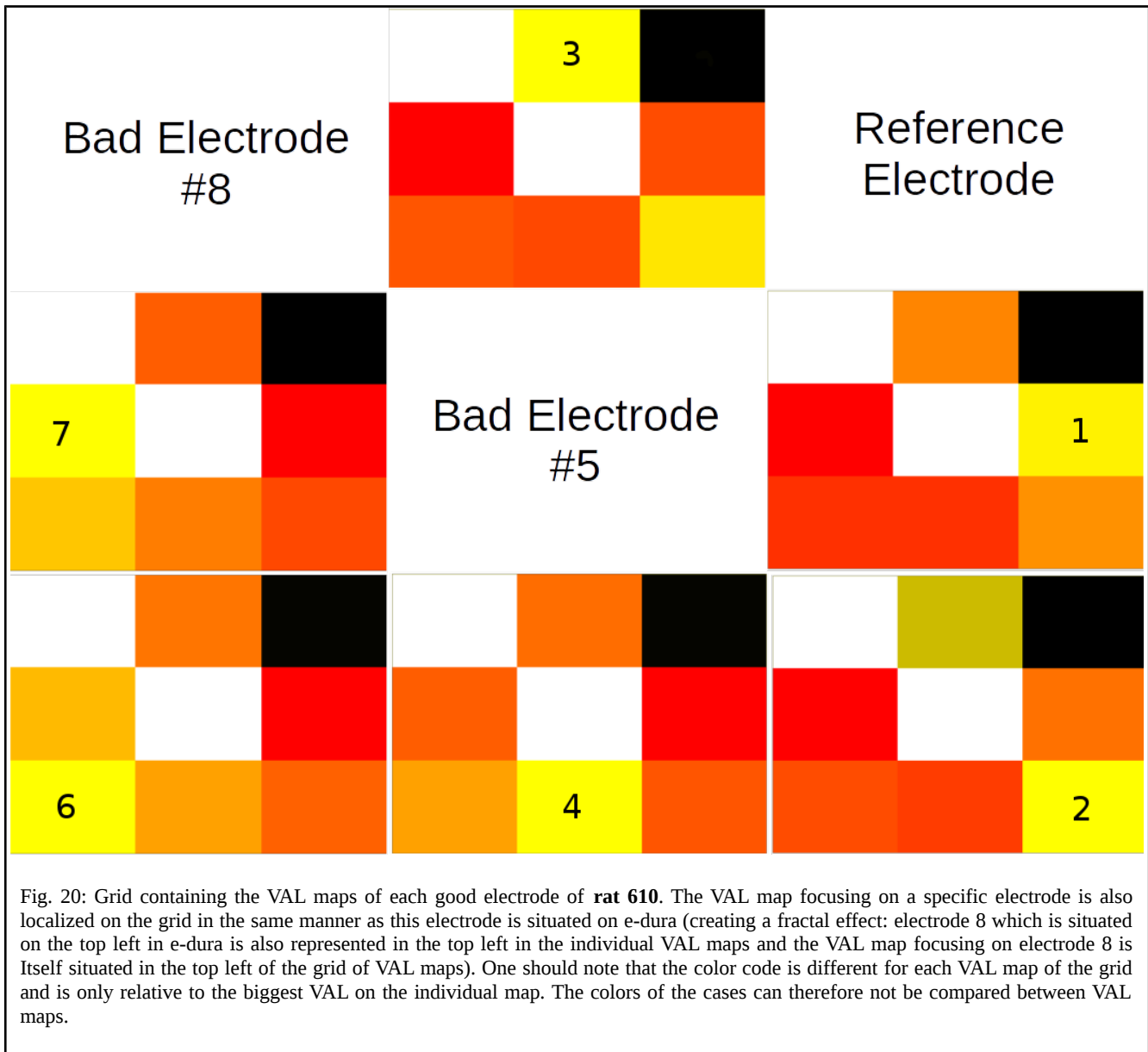


Fig. 18: The left picture displays the locations of the individual electrodes on the e-dura implant and the right picture are the mean variances of the differences between the signals (which were measured in volts) of each good electrode and electrode 6 (VAL). The respective VALs are positioned in the same manner as the individual electrodes on the e-dura picture (left). The VALs (multiplied by  $10^9$ ) are noted in the center of each corresponding case (electrode 6 corresponds to the bottom left case, electrode 5 corresponds to the central case, etc...). The color code shows the cases corresponding to smaller variances yellowish and the ones with bigger variances reddish. Electrode 6 naturally has a variance of zero with itself. The black case corresponds to the reference electrode and the white case refers to electrode 2, which was assigned as corrupted and was therefore omitted in the analysis. The data of these VALs comes from ECoG record of rat 608 made with e-dura.





## 5. Discussion

Although some analyses suffered due to a lack of data, the overall quantity of records from the various experiments could yield satisfactory results for the primary need of this thesis, which was to evaluate the potential of e-dura for BCI implementations.

### 5.1. Frequency spectra

The amplitudes of the mean frequency spectra suggest an increase in impedance from day 7 to day 21 (subsequent to e-dura implantation) followed by a decrease in impedance from day 21 to day 55 to finally reach an impedance lower than it initially was on day 7. From the results, one can postulate that the impedance probably rose between the day 1 and day 21 due to the immune reaction resulting from the implantation. This corresponds to the findings of Henle et al. (2011), who have observed an increase in impedance / Ohm of their electrodes at 1 kHz between the 3<sup>rd</sup> and the 7<sup>th</sup> day after the subdural implantation of their micro-ECoG over parts of the left motor and visual cortex. In the case of the e-dura study the impedance would have seemed to have declined between day 21 and 55. Similar results were observed by Williams et al. (2007, see Fig. 21) during their impedance study of chronically implanted intracortical microelectrode array. They detected a rise in electrode impedances peaking around day 6 following surgery that decreased to arrive close to the initial impedance level. It is plausible that a similar impedance behavior has occurred in the e-dura study. It should however be noted that the study didn't directly measure impedance. It therefore cannot be stated that changes in impedance have been measured but only suggested by this analysis.

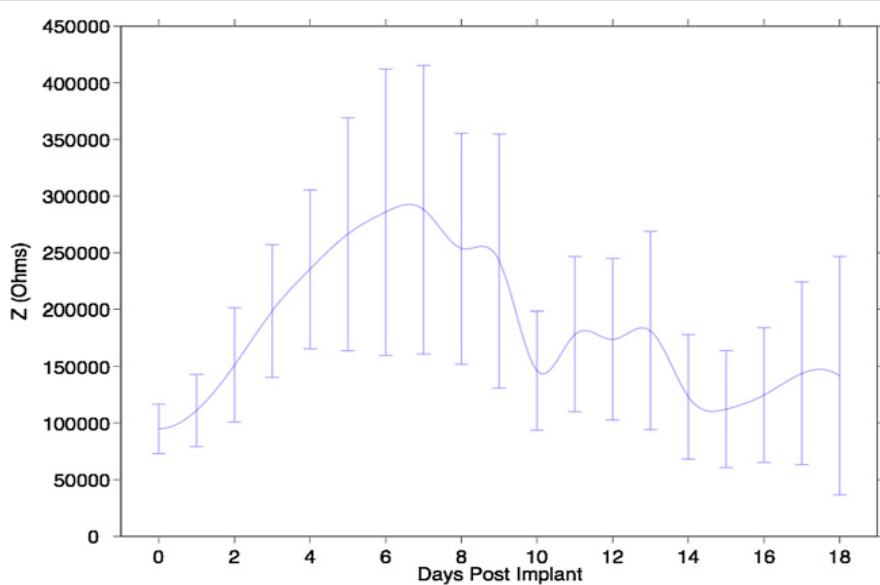


Fig. 21: Magnitude impedance (Z), measured at 1 kHz over an 18-day period post-implant. The solid line shows the mean of all of the electrodes and the error bars signify the standard deviation. This data is from 80 individual electrode sites (spanning four animals), each measured 20 times daily. (from Williams et al., 2007)

## 5.2. Spectrogram patterns

The spectrogram patterns don't accurately measure the spatial resolution. However, they can deliver information about the specificity of the signal recorded by each electrode. The individual electrodes yielded similar patterns but each contained characteristic singularities attesting the specificity of each recorded signal. It remains uncertain if the amount of data was sufficient to deliver a truly characteristic pattern of the investigated events. The start and stop patterns of each rat were averaged from between 21 and 54 spectrograms and it would be interesting to examine if the patterns would reinforce to build even more defined patterns by averaging an even bigger number of spectrograms.

Due to the shortage of occurrence, the comparison between the patterns of left and right leg stumbling cannot deliver a statistically powerful interpretation. The available data however suggest interesting differences between the two patterns. It is difficult to say if the high gamma activity band in the left foot spectrogram around  $t = -0.4s$  is part of the characteristic pattern or due to noise (see Fig. 12). The observed decrease in high gamma activity around  $t=0s$  in the right foot spectrograms of each electrode seems to be part of the pattern. Since the micro-ECoG implant was situated on the left hemisphere of the rat's motor cortex, it is expected that the pattern for right leg stumbling should be more specific than the one for the left leg. This hypothesis is supported by the observations in the 200-300 Hz range of the right foot spectrograms (see Fig. 13). This sudden change happens at the moment when the foot is at deepest in the gap of the ladder and just about to rise again. One could conjecture that this decrease in high gamma activity could be correlated with the brain signals responsible for inhibiting the further movement of the right leg. Whatever the exact purpose of this change in high gamma activity might really be, it shows us a well timed and defined pattern for the right foot that isn't visible on the pattern of the left foot. On the contrary, the increase in activity at  $t=0s$  (especially in the 100-150 Hz range) is visible on both patterns and is therefore unlikely to be directly correlated with the movement of the legs.

Although they don't bear interesting information concerning the event related characteristic spectrogram patterns, the results from all the data of rat 610 (see Fig. 14 and 15) can give us an insight into the effects of common average referencing. One can see that most of the noise related bands are present in all the spectrograms including the one of the average reference. However, the band at  $t=-1s$  in Fig. 14 and the one just before  $t=0.5s$  in Fig. 15 are only present in the average reference. When looking at Fig. 16 and 17, it seems that the average referencing technique should be successful at removing global noise from the signals of the individual electrodes. It therefore seems strange that some noise bands can be present on all spectrograms. The best explanation for this phenomena is that one electrode experienced a strong noise at some point, probably due to a bad contact with the brain, and should have therefore been labeled as corrupted but remained undetected. If this were the case, the signal of this corrupted electrode would have contributed to the common average and the noise would have been transferred onto all the other electrodes when the common average was subtracted from each electrode signal, which would explain the patterns observed. Average referencing thus seems to be as effective at removing as at adding noise to the ECoG signals. This stresses the need for an accurate and robust algorithm that can detect corrupted electrodes.

### 5.3. Variance analysis of locality

Overall the variance analysis of locality has fulfilled the expectations and has advocated the resolution and specificity of the ECoG signals recorded by e-dura. It is interesting to note that VAL is robust to corrupted common average references (CAR) and that anomalies in the VAL map can therefore only be attributed to the aberrant behavior of one of the two concerned electrodes.

$$\begin{aligned} VAL_{ij} &= \frac{1}{n} \sum_{k=1}^n \text{variance}((\text{electrode}_i^k - \text{CAR}) - (\text{electrode}_j^k - \text{CAR})) \\ &= \frac{1}{n} \sum_{k=1}^n \text{variance}(\text{electrode}_i^k - \text{electrode}_j^k) \end{aligned} \quad (2)$$

The peculiarities observed in the VAL maps are difficult to interpret because of the low number of electrodes contained on the ECoG implant and the small area covered. It seems possible that the relatively big VALs observed for electrode 8 in rat 608 (see Fig. 19) and the uncommonly small VAL between electrode 2 and 3 in rat 610 (see Fig. 20) could be due to the variability in impedance of the individual electrodes. This could lead to differences in the sensitivity of the recordings, which would distort the VALs, since it is dependent on variance. In a further study the ECoG signals should be normalized depending on the impedance of the electrodes. This method should also be applied using the recorded signals of an implant containing more electrodes. This would allow to assess if peculiarities such as the big VALs of electrode 8 of rat 608 went in all directions and would break the pattern of degrading color, or if they build island anomalies, which would have to be correlated with an unconventional recording of the concerned electrode itself. Furthermore, this would offer a better picture of how the VAL behaves between electrodes separated by bigger distances. It would also be interesting to compare the VAL maps between different types of data to see if they differ, which would be a way of measuring the consistency of the VAL method.

#### 5.4. E-dura's potential for BCI

Overall the results showed a stable ECoG signal recording capacity over time. The average amplitude of the records slightly varied, but since it could be renormalized if necessary, this wouldn't significantly impair a BCI. Furthermore Henle et al. (2011) observed that the impedance of chronic ECoG stabilizes with time, which means that if the electrical impedance variations of the electrodes were responsible for the observed changes in amplitude, these would also stabilize with time.

The mean spectrogram patterns showed that very specific signals could be recorded from the individual electrodes and the variance analysis of location supported that these variations were correlated with the locations of the electrodes. These evidences support that the e-dura implant exploited the high density of electrodes and could record very local signals. The results therefore confirm the claim that ECoG technology and especially e-dura has the potential to be used for high performance BCI (Schalk, 2010; Brunner et al., 2011).

The main concern for the chronic application of e-dura remains its safety for the implanted individual, which was emphasized by the observed damages sustained by the brains of the rats that were implanted with the device. The source of the damage however is more likely to be of surgical origin than from the implant being present on the brain surface of the rats. To investigate this claim, further *in vivo* experiments should be conducted with optimized surgical protocols.

While EEG based BCI have already been brought into the homes of users (Vaughan et al., 2006), ECoG based BCI are still far from commercial application. The most important milestone to achieve this goal remains to prove the safety of an ECoG implant over a long period of time. Since this cannot be tested in humans, it is necessary that chronic animal studies are conducted over long time periods.

#### 5.5. Future studies

Although the data analysis from the experiments was able to provide significant and insightful results, a well prepared second round of experiments could reveal itself to be even more rewarding. If such a study came to be conducted, it should take place over a prolonged period of time. 55 days is already quite long but since BCI implementations would have to stay implanted over months or years, it doesn't seem sufficient to investigate the long term safety of the technology. It would also be beneficial to conduct experiments as soon as possible after implantation of the device, in order to have a better idea of the initial condition and signals, which would be very valuable to investigate the influence of time on the implant and its recordings. Additionally, the number of electrodes on the implant should be increased since an ECoG based high performance BCI would likely necessitate more signal recordings, over a larger area of the brain. An increased number of electrodes would also offer a richer variety of possibilities for common average referencing. It might, for example, be interesting to average reference each signal with the common average of the 8 closest electrodes around the recording electrode in order to acquire the best possible resolution. More electrodes would also strengthen the results from a variance analysis of locality. With the VAL maps of implants containing a large number of electrodes, it might be possible to use the map as a tool to detect corrupted electrodes. It would be extremely useful to develop such an algorithm, capable of distinguishing between corrupted and uncorrupted electrodes with a high fidelity. Such a method would spare a lot of time for the user and would also prevent wrong conclusions due to the fallibility of human decisions. Mean spectrogram patterns could also be used in a failure detection algorithm in order to determine if corrupted electrodes remained undetected.

## 6. Acknowledgements

I would first like to express my gratitude to Prof. Stéphanie Lacour for accepting to be my supervisor during my Bachelor's thesis despite of the uncommon circumstances, in which I desired to perform this work. I am especially grateful for her requirements from me to train my writing and presentation skills in order to improve them.

A special thank goes to Arthur Hirsch for his guidance and advices during my whole thesis. Without him this project would have never existed and I am greatly thankful that he allowed me to take an active part in it. His recommendations and knowledge were always of great help and allowed me to learn a lot.

## 7. References

- Bélanger, M. and Marois, Y., 2001, *Hemocompatibility, biocompatibility, inflammatory and in vivo studies of primary reference materials low-density polyethylene and polydimethylsiloxane: A review*, J. Biomed. Mater. Res., 58: 467–477.
- Peter Brunner, Anthony L. Ritaccio, Joseph F. Emrich, Horst Bischof and Gerwin Schalk, 2011, *Rapid Communication with a “P300” Matrix Speller Using Electrocorticographic Signals (ECoG)*, Frontier in Neuroengineering, 5: 5.
- György Buzsáki, Costas A. Anastassiou and Christof Koch, 2012, *The origin of extracellular fields and currents--EEG, ECoG, LFP and spikes*, Nature Reviews Neuroscience 13, 407-420.
- Tom Carlson and José del R. Millán, 2013, *Brain–Controlled Wheelchairs: A Robotic Architecture*, IEEE Robotics and Automation Magazine, 20(1): 65 – 73.
- Elisa Castagnola, Alberto Ansaldi, Emma Maggiolini, Tamara Ius, Miran Skrap, Davide Ricci and Luciano Fadiga, 2014, *Smaller, softer, lower-impedance electrodes for human neuroprosthesis: a pragmatic approach*, Frontiers in Neuroengineering, vol. 7, article 8.
- Karen C. Cheung, Philippe Renaud, Heikki Tanila, Kaj Djupsund, 2007, *Flexible polyimide microelectrode array for in vivo recordings and current source density analysis*, Biosensors and Bioelectronics, Volume 22, Issue 8, 15 March 2007, Pages 178–1790
- Joseph Dien, 1998, *Issues in the application of the average reference: Review, critiques, and recommendations*, Behavior Research Methods, Instruments, & Computers, 30(1): 34-43.
- Eduardo Fernández, Bradley Greger, Paul A. House, Ignacio Aranda, Carlos Botella, Julio Albisua, Cristina Soto-Sánchez, Arantxa Alfaro and Richard A. Normann, 2014, *Acute human brain responses to intracortical microelectrode arrays: challenges and future prospect*, Frontiers in Neuroengineering, v. 7.
- Freeman W. J., Holmes M. D., Burke B. C. and Vanhatalo S., 2003, *Spatial spectra of scalp EEG and EMG from awake humans*, Clin. Neurophysiol., 114 1053–68.
- Walter J. Freeman, Linda J. Rogers , Mark D. Holmes, Daniel L. Silbergeld, 2000, *Spatial spectral analysis of human electrocorticograms including the alpha and gamma bands*, Journal of Neuroscience Methods, 95 111 – 121.
- Charles M. Gaona, Mohit Sharma, Zachary V. Freudenburg, Jonathan D. Breshears, David T. Bundy, Jarod Roland, Dennis L. Barbour, Gerwin Schalk and Eric C. Leuthardt, 2011, *Nonuniform High-Gamma (60 –500 Hz) Power Changes Dissociate Cognitive Task and Anatomy in Human Cortex*, The Journal of Neuroscience, February 9, 2011 • 31(6):2091–2100 • 2091.

C. Henle, M. Raab, J. G. Cordeiro, S. Doostkam, A. Schulze-Bonhage, T. Stieglitz and J. Rickert, 2011, *First long term in vivo study on subdurally implanted Micro-ECoG electrodes, manufactured with a novel laser technology*, Biomed Microdevices (2011), 13:59–68.

N. Jeremy Hill, Disha Gupta, Peter Brunner, Aysegul Gunduz, Matthew A. Adamo, Anthony Ritaccio, Gerwin Schalk, 2012, *Recording Human Electrocorticographic (ECoG) Signals for Neuroscientific Research and Real-time Functional Cortical Mapping*, J. Vis. Exp. (64), e3993.

E. Leuthardt, G. Schalk, J. Wolpaw, J. Ojemann, and D. Moran, 2004, *A brain–computer interface using electrocorticographic signals in humans*, J Neural Eng, 1(2):63–71.

Gregory A. Light, Ph.D., Lisa E. Williams, M.A., Falk Minow, Joyce Srock, Anthony Rissling, Richard Sharp, Neal R. Swerdlow, M.D., Ph.D. and David L. Braff, M.D., 2010, *Electroencephalography (EEG) and Event-Related Potentials (ERPs) with Human Participants*, Curr Protoc Neurosci., CHAPTER: Unit–6.2524.

Joseph N. Mak, Member and Jonathan R. Wolpaw, 2009, *Clinical Applications of Brain-Computer Interfaces: Current State and Future Prospects*, IEEE Rev Biomed Eng., 2: 187–199.

Gerwin Schalk, 2012, *Can electrocorticography (ECoG) support robust and powerful brain–computer interfaces?*, Frontier in Neuroengineering, 3: 9.

Gerwin Schalk, 2012, BCIs That Use Electrocorticographic Activity, in Jonathan Wolpaw and Elizabeth Winter Wolpaw, *Brain–Computer Interfaces: Principles and Practice*, Oxford University Press, New York, 406 p.

Fernando Lopez da Silva and Ab Van Rotterdam, 2005, Biophysical Aspects of EEG and Magnetoencephalogram Generation, in Ernst Niederheimer and Fernando Lopez da Silva, *Electroencephalography: Basic Principles, Clinical Applications and Related Fields*, Lippincott Williams & Wilkins, Philadelphia, PA, 1286 p.

M. Smith, K. Weaver, T. Grabowsky, and F. Darvas, Utilizing High Gamma (HG) Band Power Changes as a Control Signal for Non-Invasive BCI, in Christoph Guger, Brendan Z. Allison and Günter Edlinger, *Brain-Computer Interface Research: A State-of-the-Art Summary*, Springer, Heidelberg, New York, Dordrecht, London, 123 p.

Theresa M. Vaughan, Dennis J. McFarland, Gerwin Schalk, William A. Sarnacki, Dean J. Krusinski, Eric W. Sellers, and Jonathan R. Wolpaw, 2006, *The Wadsworth BCI research and development program: at home with BCI*, IEEE Transactions on Neural Systems and Rehabilitation Engineering, vol. 14, no. 2.

Justin C. Williams, Joseph A. Hippensteel, John Dilgen, William Shain and Daryl R. Kipke, 2007, *Complex impedance spectroscopy for monitoring tissue responses to inserted neural implants*, J. Neural Eng. 4 (2007) 410–423.

J. Adam Wilson, Christoph Guger, Gerwin Schalk, 2012, BCI Hardware and Software, in Jonathan Wolpaw and Elizabeth Winter Wolpaw, Brain–Computer Interfaces: Principles and Practice, Oxford University Press, New York, 406 p.

Andrew J Woolley, Himanshi A Desai and Kevin J Otto, 2013, *Chronic intracortical microelectrode arrays induce non-uniform, depth-related tissue responses*, J. Neural Eng. 10 026007.

Zhuolin Xiang, Shih-Cheng Yen, Ning Xue, Tao Sun, Wei Mong Tsang, Songsong Zhang, Lun-De Liao, Nitish V Thakor and Chengkuo Lee, 2014, *Ultra-thin flexible polyimide neural probe embedded in a dissolvable maltose-coated microneedle*, J. Micromech. Microeng. 24 065015.

## 8. List of Figures

Figure 1: Tissue layers around the brain and recording sites of EEG and ECoG electrodes, Schalk G. and Leuthard E. C., 2011, *Brain-Computer Interfaces Using Electrocorticographic Signal*, IEEE Reviews in Biomedical Engineering, vol. 4.

Figure 2: Flexible e-dura implant designed and manufactured by Arthur Hirsch.

Figure 3: Low pass filtered, raw ECoG signal example of the 8 electrodes of the flexible e-dura micro-ECoG implant displaying how corrupted electrodes were detected.

Figure 4: Low pass filtered, common average referenced ECoG signal example of the uncorrupted electrodes of the flexible e-dura micro-ECoG implant.

Figure 5: Comparison of the frequency spectra from the data of rat 610 collected 7, 21 or 55 days after the implantation of the e-dura implant.

Figure 6: Comparison of the frequency spectra from the data of rat 608 collected 7, 21 or 55 days after the implantation of the e-dura implant.

Figure 7: Comparison of the frequency spectra from the passive data of rat 608 collected 7, 21 or 55 days after the implantation of the e-dura implant.

Figure 8: Comparison of the frequency spectra from the active data of rat 608 collected 7, 21 or 55 days after the implantation of the e-dura implant.

Figure 9: Comparison of the frequency spectra from the active data of rat 10 collected 7, 21 or 55 days after the implantation of the e-dura implant.

Figure 10: Characteristic spectrogram patterns of rat 608 starting to run.

Figure 11: Characteristic spectrogram patterns of rat 608 stopping to run.

Figure 12: Characteristic spectrogram patterns of rat 608 stumbling with the left foot.

Figure 13: Characteristic spectrogram patterns of rat 608 stumbling with the right foot.

Figure 14: Characteristic spectrogram patterns of rat 610 starting to run, made from all available data.

Figure 15: Characteristic spectrogram patterns of rat 610 stopping to run made from all available data.

Figure 16: Characteristic spectrogram patterns of rat 610 starting to run made with a set of data, from which all spectrograms containing bands of noise have been removed prior to the computation of the patterns.

Figure 17: Characteristic spectrogram patterns of rat 610 stopping to run made with a set of data, from which all spectrograms containing bands of noise have been removed prior to the computation of the patterns.

Figure 18: Example of a VAL map explained.

Figure 19: Grid of VAL maps for each uncorrupted electrode of rat 608.

Figure 20: Grid of VAL maps for each uncorrupted electrode of rat 610.

Fig. 21: Impedance plot of an intracortical electrode array over 18 days, Justin C. Williams, Joseph A. Hippенстейл, John Dilgen, William Shain and Daryl R. Kipke, 2007, *Complex impedance spectroscopy for monitoring tissue responses to inserted neural implants*, J. Neural Eng. 4 (2007) 410–423.